



Universiteit
Leiden
The Netherlands

Quantum dot microcavity control of photon statistics

Snijders, H.J.

Citation

Snijders, H. J. (2018, December 20). *Quantum dot microcavity control of photon statistics. Casimir PhD Series*. Retrieved from <https://hdl.handle.net/1887/67538>

Version: Not Applicable (or Unknown)

License: [Licence agreement concerning inclusion of doctoral thesis in the Institutional Repository of the University of Leiden](#)

Downloaded from: <https://hdl.handle.net/1887/67538>

Note: To cite this publication please use the final published version (if applicable).

Cover Page



Universiteit Leiden



The handle <http://hdl.handle.net/1887/67538> holds various files of this Leiden University dissertation.

Author: Snijders, H.J.

Title: Quantum dot microcavity control of photon statistics

Issue Date: 2018-12-20

Chapter 5

Observation of the unconventional photon blockade

We observe the unconventional photon-blockade effect in QD cavity QED, which, in contrast to conventional photon blockade, operates in the weak coupling regime. A single QD transition is simultaneously coupled to two orthogonally polarized optical cavity modes, and by careful tuning of the input and output state of polarization, the unconventional photon-blockade effect is observed. We find a minimum second-order correlation $g^{(2)}(0) \approx 0.37$ which corresponds to $g^{(2)}(0) \approx 0.005$ when corrected for detector jitter, and observe the expected polarization dependency and photon bunching and anti-bunching very close-by in parameter space, which indicates the abrupt change from phase to amplitude squeezing.

This Chapter has been published in *Physics Review Letters* 121, 043601 (2018) [84].

5.1 Introduction

A two-level system strongly coupled to a cavity results in polaritonic dressed states with a photon-number dependent energy. This dressing gives rise to the photon-blockade effect [85, 21] resulting in photon-number dependent transmission and reflection, enabling the transformation of incident coherent light into specific photon-number states such as single photons. Single-photon sources are a crucial ingredient for various photonic quantum technologies ranging from quantum key distribution to optical quantum computing. Such sources are characterized by a vanishing second-order auto-correlation $g^{(2)}(0) \approx 0$ [86].

In the strong coupling regime, where the coupling between the two-level system and the cavity is larger than the cavity decay rate ($g > \kappa$) [23], photon blockade has been demonstrated in atomic systems [57], QDs in photonic crystal cavities [62], and circuit QED [87, 88]. At the onset of the weak coupling regime ($g \approx \kappa$), it has been shown that by detuning the dipole transition frequency with respect to the cavity resonance, photon blockade can still be observed [66]. However, moving further into the weak coupling regime ($g < \kappa$) which is much easier to achieve [89, 5] (in particular if one aims for a small polarization mode splitting), conventional photon blockade is no longer possible because the energy gap between the polariton states vanishes. Nevertheless, also in the weak coupling regime, the two-level system enables photon number sensitivity, which has recently enabled high-quality single-photon sources using polarization postselection [4, 2, 3] or optimized cavity in-coupling [90]. We focus in this chapter on resonantly excited systems. In 2010, Liew and Savona introduced the concept of the unconventional

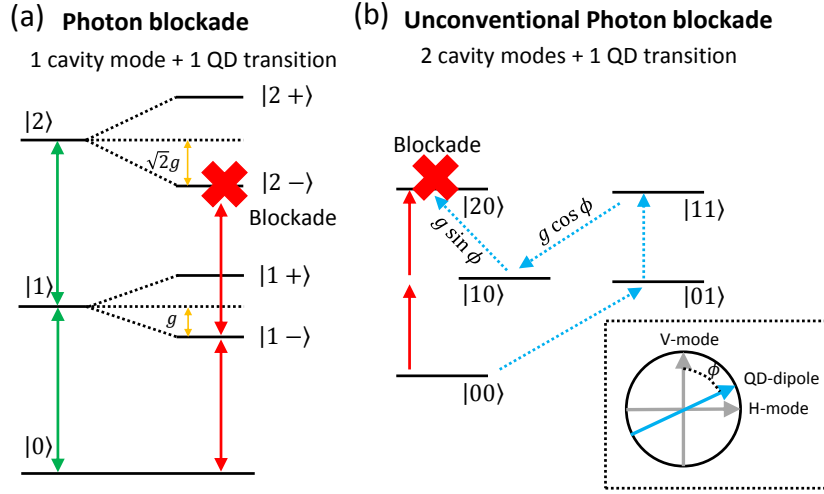


Figure 5.1: Removal of the 2-photon component in conventional photon blockade by the anharmonicity of the Jaynes–Cummings ladder (a). In the unconventional photon blockade (b, adapted from [91]), two excitation pathways (red and blue arrows) destructively interfere. The state $|ij\rangle$ corresponds to (i, j) photons in the (H, V) polarized microcavity modes. The QD is coupled (coupling constant g) to both cavity modes due to an orientational mismatch of its dipole (angle ϕ , see inset).

photon blockade (UPB) [92, 93] which operates with arbitrarily weak nonlinearities. It was first investigated for Kerr nonlinearities [94, 95], then for $\chi^{(2)}$ nonlinearities [96] and the Jaynes–Cummings [91, 97] system which we focus on here. Both the conventional and unconventional photon-blockade effect result in transmitted light with vanishing photon auto-correlation $g^{(2)}(0) < 10^{-2}$ [94, 98], however, the underlying physical mechanisms are completely different, see Fig. 5.1. In the strong coupling regime, the unevenly spaced levels of the dressed spectrum prevent reaching the two-photon state for a particular laser frequency [red arrows in Fig. 5.1(a)]. Moreover, the probabilities of having $N > 1$ photons in the system are all suppressed with respect to those of a classical state with the same average photon number. In the unconventional photon blockade instead [Fig. 5.1(b)], only the probability of having $N = 2$ photons is suppressed. The sub-Poissonian character then arises because, for the chosen pump amplitude, the average photon number – and thus the probabilities of $N > 2$ photons – are very small. A possible explanation of the reduced $N = 2$ probability is given in terms of the interference between two excitation pathways to the $N = 2$ photon state, which can be destructive thanks to the small energy shift of the two-photon state induced by the weak nonlinearity [91, 99]. An equivalent alternative explanation (discussed below) was proposed in terms of an optimal interplay between squeezing and displacement of the cavity field [100].

We investigate here a single semiconductor QD in an optical microcavity where a single linearly-polarized QD dipole transition is coupled to the two linearly polarized cavity modes due to an orientational mismatch of the QD dipole with respect to the cavity axes [angle ϕ , see inset Fig. 5.1(b)]. Since the unconventional photon blockade operates in the low mean-photon-number regime, Fig. 5.1(b) shows only the $N = 0..2$ photon Fock states. Further, we show only one particular excitation pathway (blue), many more involving internal cavity coupling exist but do not qualitatively change the interpretation. More specifically, we rely here on the input- output tuning scheme described in detail in [93, 94], here realized via the polarization degree of freedom, which is an extension of the original UPB proposal [91, 92]. As a result the interference of different excitation pathways with and without involvement of the photon-number sensitive QD transition can be tuned such that the two-photon component is suppressed.

5.2 Device and experimental setup

The sample for this experiment consist of a layer of self-assembled InAs/GaAs QDs embedded in a micropillar cavity (maximum Purcell factor $F_p = 11.2$) grown by molecular beam epitaxy [73]. The QD layer is embedded in a P–I–N junction, separated by a 27 nm thick tunnel barrier from the electron reservoir to enable tuning of the QD resonance frequency by the quantum-confined Stark effect. Due to the QD fine-structure splitting, we need to consider only one QD transition, which interacts with both the H and V cavity modes.

We model our system using a Jaynes–Cummings Hamiltonian in the rotating wave approximation with $g \ll \kappa$. The Hamiltonian for two cavity modes and one QD transition

driven by a continuous-wave laser is written as

$$\begin{aligned}
H = & \left(\omega_L - \omega_c^V\right) \hat{a}_V^\dagger \hat{a}_V + \left(\omega_L - \omega_c^H\right) \hat{a}_H^\dagger \hat{a}_H \\
& + \left(\omega_L - \omega_{QD}\right) \hat{\sigma}^\dagger \hat{\sigma} + g \left(\hat{\sigma} \hat{b}^\dagger + \hat{\sigma}^\dagger \hat{b}\right) \\
& + \eta_H \left(\hat{a}_H + \hat{a}_H^\dagger\right) + \eta_V \left(\hat{a}_V + \hat{a}_V^\dagger\right).
\end{aligned} \tag{5.1}$$

ω_c^H and ω_c^V are the resonance frequencies of the linearly polarized cavity modes, \hat{a}_H^\dagger and \hat{a}_V^\dagger the photon creation operators, ω_{QD} is the QD resonance frequency, and $\hat{\sigma}^\dagger$ the exciton creation operator. $\hat{b} = \hat{a}_V \cos \phi + \hat{a}_H \sin \phi$ is the cavity photon annihilation operator along the QD dipole orientation, and ϕ is the relative angle. In our case the angle is $\phi = 94^\circ$, which means that the H-cavity mode couples better to the exciton transition. η_H and η_V are the amplitudes of the incident coherent light coupling to the H and V cavity modes. For numerical simulations, we add relaxation of the cavity modes and dephasing of the QD transition and solve the corresponding quantum master equation [37, 38, 5], add the output polarizer and calculate the mean photon number and second-order correlation function. All theoretically obtained $g^{(2)}(\tau)$ data is convolved with the detector response (530 ps) to match the experimental conditions.

In Fig. 5.2(a) we show false color plots of the cavity transmission as a function of laser frequency and QD energy. The QD energy is tuned by altering the bias voltage which modifies the quantum confined Stark effect. The input polarization is set such that we excite only one cavity mode. A cross section taken at the dashed line in (a) is shown in Fig. 5.2(b). From the fit to the theoretical model we obtain the cavity decay rate $\kappa = 60 \pm 3 \text{ ns}^{-1}$, the QD-cavity coupling constant $g = 14 \pm 0.4 \text{ ns}^{-1}$, the population relaxation rate $\gamma_{||} = 1.0 \pm 0.4 \text{ ns}^{-1}$, the pure dephasing rate $\gamma^* = 0.2 \pm 0.4 \text{ ns}^{-1}$ and the total dephasing rate $\gamma = \frac{\gamma_{||}}{2} + \gamma^* = 0.7 \text{ ns}^{-1}$.

In an additional measurement we keep the QD energy constant and rotate the input polarization, see Fig. 5.2(c). By fitting the data for several incident polarization orientations (and keeping κ , $\gamma_{||}$, γ^* and g constant), we obtain the QD fine-structure splitting $\Delta f_{QD} = 2.4 \pm 0.1 \text{ GHz}$, the cavity polarization splitting $\Delta f_{cav} = 10 \pm 0.1 \text{ GHz}$, and the angle between the QD and cavity polarization basis $\phi = 94^\circ \pm 2^\circ$. The resulting theoretically calculated transmission in Fig. 5.2(d) shows excellent agreement with the experimental data in Fig. 5.2(c).

In summary the simulation parameters used to produce the explanatory Fig. 5.4 were $\kappa = 60 \text{ ns}^{-1}$, $g = 14 \text{ ns}^{-1}$, $\gamma_{||} = 1.0 \text{ ns}^{-1}$, $\gamma^* = 0.0 \text{ ns}^{-1}$, $\Delta f_{cav} = 0 \text{ GHz}$, $\phi = 94^\circ$, and $\langle n_{in} \rangle = 0.01$, i.e., without dephasing and cavity mode splitting. For Fig. 5.5 where theory is compared to experiment, we use the full set (including pure dephasing): $\kappa = 60 \text{ ns}^{-1}$, $g = 14 \text{ ns}^{-1}$, $\gamma_{||} = 1.0 \text{ ns}^{-1}$, $\gamma^* = 0.2 \text{ ns}^{-1}$, $\Delta f_{cav} = 10 \text{ GHz}$, $\phi = 94^\circ$ and $\langle n_{in} \rangle = 0.06$. Here $\langle n_{in} \rangle$ is the incident mean photon number.

From the device parameters we see that the QD fine-structure splitting of 2.4 GHz is much larger than the QD linewidth (FWHM) of $2\frac{\gamma}{2\pi} \approx 0.2 \text{ GHz}$; therefore we can focus on one QD transition only as long as a narrow-linewidth laser is used. We have confirmed this by comparing numerical simulations with one and two fine-structure split QD transitions, where equal transmission amplitudes and photon correlations are obtained. Finally, there could be non-energy preserving and/or non-polarization preserving effects, such as phonon-assisted Raman-type transitions between the two fine-structure

split exciton states. This, however, would lead to a reduced interference of incident laser light and QD resonance fluorescence, which would imply a reduced dip depth in a simple transmission scan, this is not the case [Fig. 5.2(b)].

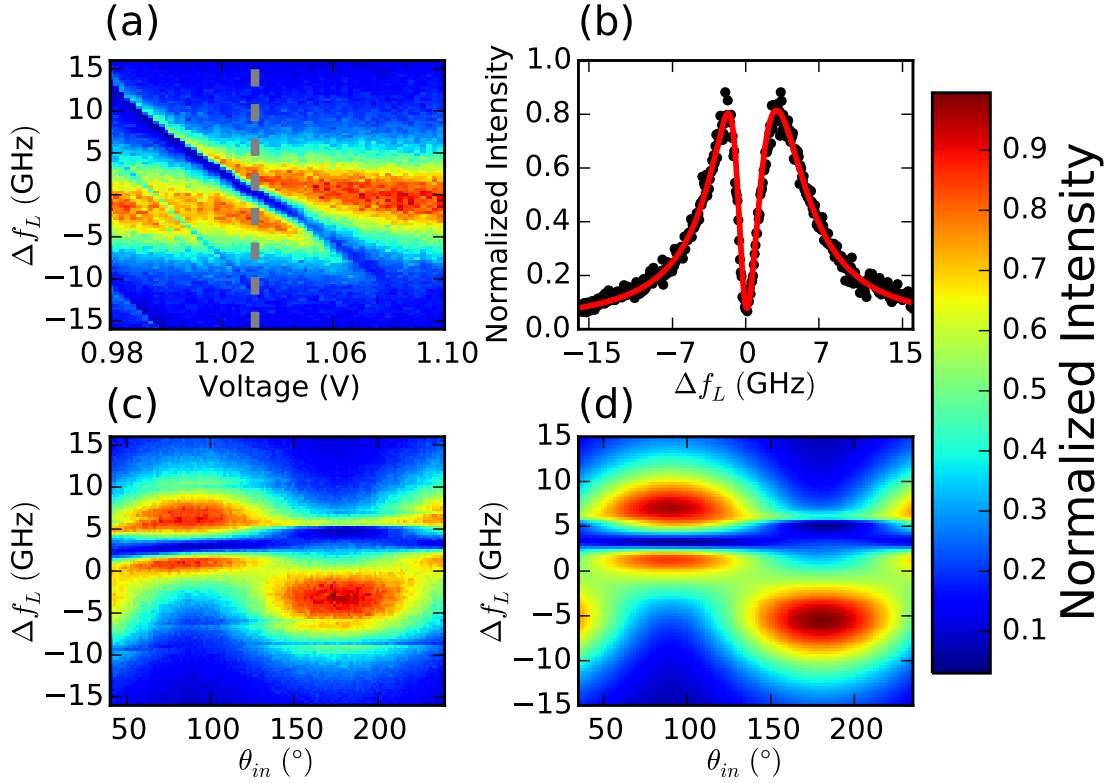


Figure 5.2: Characterization of the QD cavity-QED device by cavity transmission measurements: Cavity transmission as a function of laser frequency and QD bias voltage (a), corresponding cross-section at the dashed line (b), and experimental (c) and theoretical (d) laser frequency – incident linear polarization orientation scans of the cavity transmission.

Fig. 5.3 shows the experimental setup. For polarization control, we use exclusively Glan-type polarizers and calibrated zero-order waveplates. Light from a scanning laser is polarized, and then coupled with a 0.4 NA microscope objective into the fundamental mode of the microcavity. The device is on a cold finger at 5 K in a low-vibration closed-cycle cryostat with 3-axes piezo control for fine positioning. The transmitted light is collected using also a 0.4 NA microscope objective; motorized waveplates in combination with a fixed linear polarizer are used to select a specific state of polarization. With a non-polarizing beamsplitter and two single-photon detectors we then record photon counts and photon auto correlations.

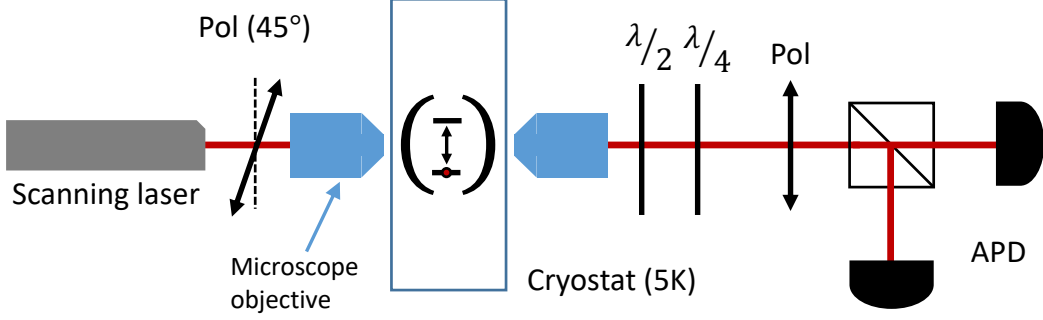


Figure 5.3: Sketch of the experimental setup. Pol: polarizer, APD: single-photon counting avalanche photodiode.

5.3 Results

Fig. 5.4 shows how the second-order correlation $g^{(2)}(\tau = 0)$ of the transmitted photons depends on the linear input and linear output polarization angle. In all current single-photon sources with a QD in a cavity [2, 3, 4], only one cavity mode is excited with the laser, and by using a crossed polarizer, single photons are obtained in the orthogonal mode. This condition is indicated with arrow A in Fig. 5.4. By exciting both cavity modes and selecting an appropriate output polarization state such as indicated by arrow B, it is also possible to obtain single photons; this is where the unconventional photon blockade can be observed.

Now, we investigate more closely region B of Fig. 5.4, where both cavity modes are excited ($\theta_{in} = 45^\circ$). Furthermore, we add the experimentally unavoidable polarization splitting of the H and V cavity modes which is 10 GHz for the device under investigation. Furthermore, we vary the detected output polarization in the most general way, by introducing $\lambda/2$ and $\lambda/4$ wave plates before the final polarizer in the transmission path. As simplified experimental setup is sketched in the inset of Fig. 5.5(b). Fig. 5.5(b) shows how this polarization projection affects the mean photon number $\langle n_{out} \rangle$, for $\langle n_{in} \rangle = \left(\frac{\eta_H + \eta_V}{\kappa} \right)^2 = 0.06$ in the simulation and in the experiment [Fig. 5.5(a)]. This region is highly dependent on the cavity splitting and the QD dipole angle, careful determination of the parameters allows us to obtain good agreement to experimental data [Fig. 5.5(a)]. In this low mean photon-number region, the second-order correlation $g^{(2)}(0)$ shows a non-trivial behavior as a function of the output polarization state, shown in Fig. 5.5(c, experiment) and (d, theory): First, we observe the expected unconventional photon blockade anti-bunching (blue region). The experimentally measured minimum $g^{(2)}(0)$ is 0.37 ± 0.04 , which is limited by the detector response function. The theoretical data which takes the detector response into account agrees very well to the experimental data and predicts a bare $g^{(2)}(0) \approx 0.005$. Second, we find that, close-by in parameter space, there is a region where bunched photons are produced. This enhancement of the two-photon probability happens via constructive interference leading to phase squeezing. Theoretical and experimental data show good agreement, we attribute the somewhat more extended antibunching region to long-time drifts of the device position during the course of the experiment (10 hours).

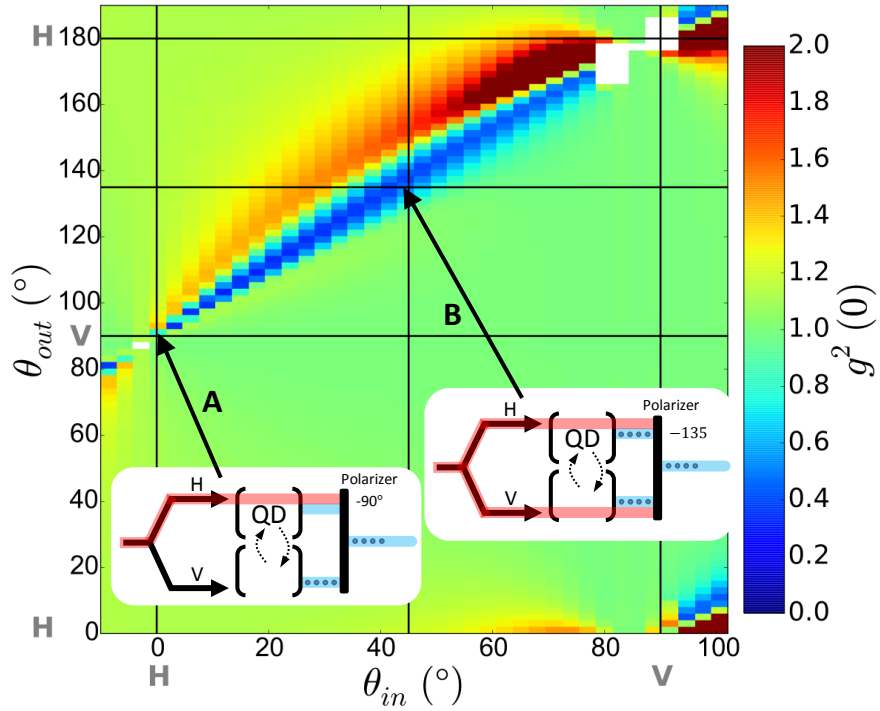


Figure 5.4: False color plot of the theoretically calculated $g^{(2)}(0)$ convolved with the detector response as a function of the incident and detected linear polarization orientation. Arrow A indicates the condition where most single-photon sources operate: the system is excited in the H-cavity mode and the single photons are detected in the V-cavity mode. Arrow B shows the case where single photons are created using the unconventional photon blockade. White pixels indicate that the simulation has failed due to extremely low photon numbers. The model parameters are given in section 5.2.

In Fig. 5.5(e) and 5.5(f) we show the two-time correlation function $g^{(2)}(\tau)$ for the two cases indicated by the arrows. The observed width and height of the anti-bunching and bunching peak predicted by the theory is in agreement with the observed experimental data. The exact shape of the correlation function in Fig. 5.5(e) is very sensitive to non-ideal effects such as energy fluctuations of the QD, which is why the functional form of the theoretical $g^{(2)}(\tau)$ (blue line Fig. 5.5) is a bit different compared to the experiment. For two coupled Kerr resonators in the UPB regime, one observes oscillations in $g^{(2)}(\tau)$ when collecting the output of only one of the cavities [92]. During finalizing this research, a manuscript describing a first observation of this effect has appeared [101]. In our case, these oscillations are absent because the system works mostly as a unidirectional dissipative coupler [102], and the photon field behind the output polarizer contains contributions from both cavities modes, which suppresses the oscillations in $g^{(2)}(\tau)$.

5.4 Discussion

An alternative way to understand the unconventional photon blockade is in terms of Gaussian squeezed states [100]: For any coherent state $|\alpha\rangle$, there exists an optimal squeeze parameter ξ that minimizes the two-photon correlation $g^{(2)}(0)$, which can be made vanishing for weak driving fields. We find that, even with a small amount of squeezing, it is possible to significantly reduce the 2-photon distribution and minimize $g^{(2)}(0)$ for low mean photon numbers. A Gaussian squeezed state is produced from vacuum via $D(\alpha)S(\xi)|0\rangle = |\alpha, \xi\rangle$. Here S is the squeeze operator with $\xi = r \exp^{i\theta}$ ($0 \leq r < \infty$, $0 \leq \theta \leq 2\pi$). D is the displacement operator, and the complex displacement amplitude $\alpha = \bar{\alpha} \exp^{i\vartheta}$ ($0 \leq \bar{\alpha} < \infty$, $0 \leq \vartheta \leq 2\pi$). For $\theta = \vartheta = 0$, we can calculate the two-photon probability in the small- α (low mean-photon-number) limit as

$$| \langle 2 | D(\alpha)S(\xi) | 0 \rangle |^2 \approx (\bar{\alpha}^2 - r)^2 / 2, \quad (5.2)$$

using a Taylor expansion. We see that, in order to obtain a vanishing two-photon probability, the squeeze parameter r needs to be equal to $\bar{\alpha}^2$ which is the mean photon number. By defining the amount of quadrature squeezing as $\langle (\Delta X_1)^2 \rangle = \frac{1}{4} e^{-2r}$ and considering a $\langle n_{out} \rangle \approx 0.004$ (Fig. 5.5(a)), this condition leads to $10 \log_{10}(e^{-0.008}) = -3 \times 10^{-2}$ dB squeezing. Interestingly, this result means that, for a weak coherent state, only a very small amount of squeezing is needed to make $g^{(2)}(0)$ drop to nearly zero.

In Fig. 5.6 we show further analysis of the theoretical calculations for the experimental state produced by the unconventional photon blockade as indicated by arrow D in Fig. 5.5(c) and (d). In agreement with Eq. 5.2 we observe that the two-photon state in the photon-number distribution shown in Fig. 5.6(a) is suppressed. By the same mechanism that suppresses the two-photon state one also expects to see an increase of the three photon component [93]. The increase of P_3 is not observed here because of the low mean photon number. From the photon-number variance given in Fig. 5.6(b), we observe that the state is amplitude squeezed. By moving from the region of arrow C to D in Fig. 5.5(d), the observed state switches from a phase-squeezed to an amplitude-squeezed state, which is a clear signature of the unconventional photon-blockade effect [93].

Finally, we discuss whether the UPB effect can be used to enhance the performance of single-photon sources, and in particular their efficiency. Traditionally, the QD is excited

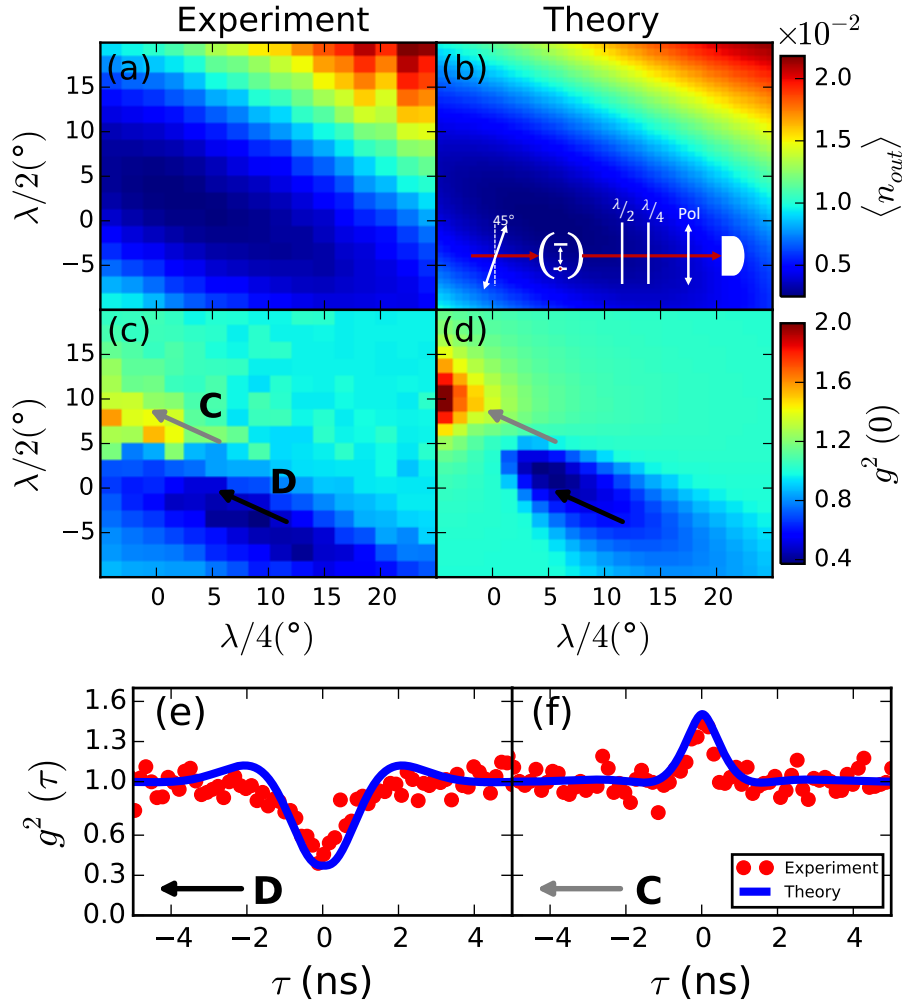


Figure 5.5: False color plots of $\langle n_{out} \rangle$ and $g^{(2)}(0)$ as a function of the orientation of the $\lambda/2$ and $\lambda/4$ wave plate in the transmission path. (a) $\langle n_{out} \rangle$ is the mean photon number in a given polarization basis at the output. At 0° the linear polarized incoming light is parallel to the fast axis of both wave plates. (b) corresponding theory to (a) with as inset a sketch of the experimental setup. (c) and (d) experimental and theoretical $g^{(2)}(0)$. (e) and (f) show $g^{(2)}(\tau)$ for the (anti) bunching region indicated by arrows C (D) in Fig. 5.5(c) and (d). The red dots are measured data and the blue line is the theoretically obtained $g^{(2)}(\tau)$ convolved with the detector response. The exact theoretical parameters are given in section 5.2.

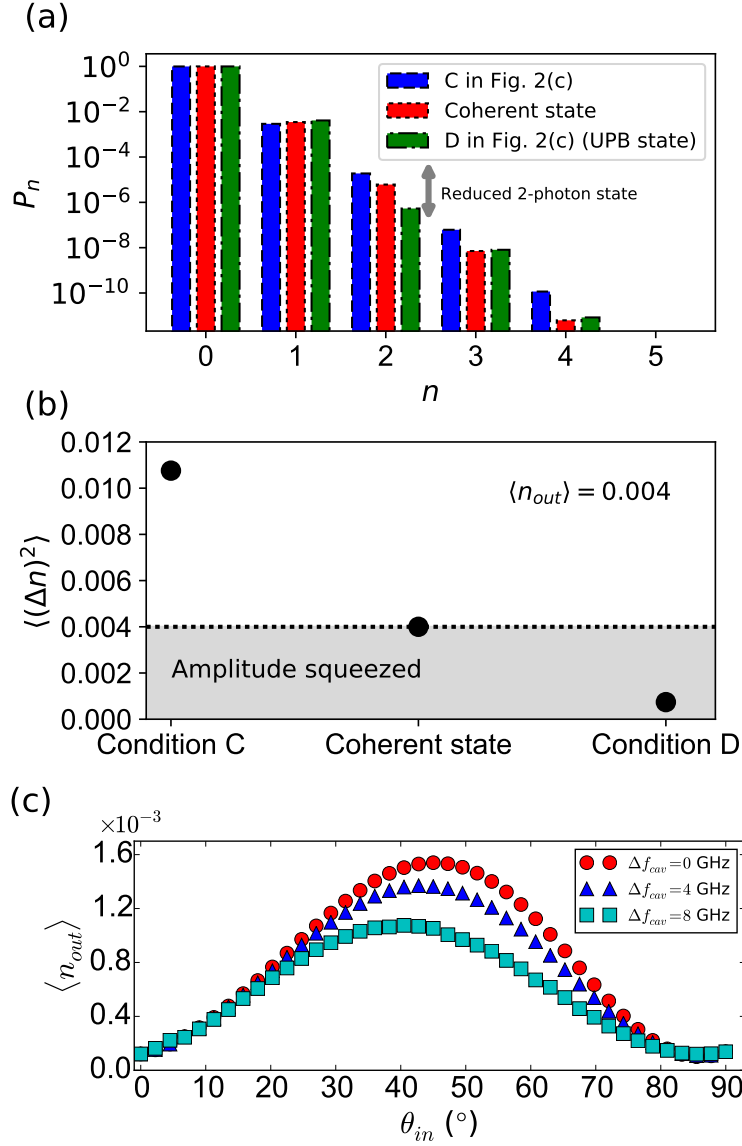


Figure 5.6: (a) Calculated photon-number distribution of a coherent state and for the condition indicated by the arrow C and D in Fig. 5.4(c). (b) The calculated photon-number variance for the states presented in (a) showing amplitude squeezing in the region where we observe the unconventional photon blockade. (c) Mean photon number $\langle n_{out} \rangle$ as a function of input polarization. We see that a large improvement of the single-photon efficiency can be obtained by exploiting the UPB effect. The simulation is performed for three cavity splittings (Δf_{cav}) showing that the enhancement is largest in a polarization degenerate cavity.

by one linearly polarized cavity mode and photons are collected via the orthogonal mode. In our experiment, the QD excitation probability is $1 - \cos(4^\circ) \approx 0.0024$, and, once excited, it has $1 - 0.0024$ chance to emit into the collection cavity mode, which leads to a low total efficiency. In the unconventional photon-blockade regime, arrow B in Fig 5.4, this efficiency is higher. To further explore this, we show in Fig. 5.6(c) the mean photon number $\langle n_{out} \rangle$ as a function of the input polarization with constant input laser power $\langle n_{in} \rangle = 0.06$ (the polarization output state is chosen such that $g^{(2)}(0) \approx 0$). We see that, by rotating the input polarization from 0° to 45° , the output mean photon number can be increased by approximately a factor 10. The simulation is done for various cavity splittings Δf_{cav} which shows that increasing the cavity splitting reduces this enhancement. We conclude that, in the low mean-photon-number regime, the UPB effect can be used to increase the efficiency of a single-photon source.

In conclusion, we have experimentally observed the unconventional photon-blockade effect using a single QD resonance coupled to two orthogonally-polarized cavity modes. We find the expected drop in $g^{(2)}(0)$, but additionally and very close in parameter space, we also find that the transmitted light statistics can be tuned from anti-bunched to bunched, all in good agreement to theoretical models and simulations. In contrast to conventional photon blockade, no energy splitting of the polariton resonances is required, allowing to obtain $g^{(2)}(0) \approx 0$ even with weak nonlinearities. Finally, under certain conditions, we find that the unconventional photon-blockade effect can increase the efficiency of single-photon sources.

